

# **Low Cost, High Performance Actuators for Dynamic Robots**

by

Benjamin G. Katz

Submitted to the Department of Mechanical Engineering  
in partial fulfillment of the requirements for the degree of

Bachelor of Science in Mechanical Engineering

at the

MASSACHUSETTS INSTITUTE OF TECHNOLOGY

June 2016

© Massachusetts Institute of Technology 2016. All rights reserved.

Author .....  
Department of Mechanical Engineering  
May 18, 2016

Certified by .....  
Sangbae Kim  
Associate Professor  
Thesis Supervisor

Accepted by .....  
Anette Hosoi  
Professor of Mechanical Engineering, Undergraduate Officer



# **Low Cost, High Performance Actuators for Dynamic Robots**

by

Benjamin G. Katz

Submitted to the Department of Mechanical Engineering  
on May 18, 2016, in partial fulfillment of the  
requirements for the degree of  
Bachelor of Science in Mechanical Engineering

## **Abstract**

The recent growth of the remote control airplane and drone market has created great availability of extremely cheap, yet very power and torque dense electric motors. However, these motors have for the most part been neglected by the robotics community. This thesis documents the development of a hardware, firmware, and controls platform for using these motors in robotics applications - specifically for running robots. A sampling of these motors were characterized, and appropriate position sensing, power electronics and field-oriented motor control systems for torque, position, and impedance control of the motors was developed. Additionally, a module which combines motor, electronics, and single-stage planetary gearset was designed and fabricated. For demonstration, a pair of these motor-controller- gearbox modules were incorporated in a 2-degree- of-freedom leg capable of jumping and controlling its joint impedances.

Thesis Supervisor: Sangbae Kim  
Title: Associate Professor



# Contents

<b>1</b>	<b>Introduction</b>	<b>11</b>
1.1	Motivation . . . . .	11
1.2	Scope . . . . .	11
1.3	Thesis Organization . . . . .	12
<b>2</b>	<b>Motor Characterization and Selection</b>	<b>15</b>
2.1	Testing Methodology . . . . .	15
2.2	Measurement and Characterization . . . . .	16
2.2.1	Turnigy 5208 Gimbal Motor . . . . .	16
2.2.2	Turnigy 5010 Multistar Elite . . . . .	17
2.2.3	Gartt ML 5208 . . . . .	18
2.2.4	Turnigy Multistar 4830 . . . . .	19
2.3	Testing Conclusions and Motor Selection . . . . .	20
<b>3</b>	<b>Motor Control Hardware</b>	<b>23</b>
3.1	Inverter . . . . .	23
3.2	Position and Velocity Sensing . . . . .	26
3.2.1	Hardware . . . . .	26
3.2.2	Velocity Measurement Technique . . . . .	26
<b>4</b>	<b>Motor Control</b>	<b>29</b>
4.1	Field Oriented Control Implementation . . . . .	29
4.1.1	Current Regulator Design . . . . .	30

4.2	Torque and Impedance Control . . . . .	32
4.3	Measurement of Cogging Torque and Torque Ripple . . . . .	33
<b>5</b>	<b>Motor Module Design</b>	<b>37</b>
<b>6</b>	<b>Two Degree of Freedom Leg</b>	<b>41</b>
<b>7</b>	<b>Summary and Conclusion</b>	<b>45</b>
7.1	Design Summary . . . . .	45
7.2	Improvements and Future Work . . . . .	45

# List of Figures

1-1	Motor module and 2-DOF Leg . . . . .	12
2-1	Selection of motors tested. . . . .	15
2-2	Turnigy 5208 Gimbal Motor . . . . .	16
2-3	5208 Gimbal Motor back-EMF waveform . . . . .	17
2-4	Turnigy Multistar Elite 5010 . . . . .	17
2-5	MultistarElite 5010 back-EMF waveform . . . . .	18
2-6	Gartt 5208 Motor . . . . .	18
2-7	Gartt 5208 back-EMF waveform . . . . .	19
2-8	Turnigy Multistar 4830 . . . . .	19
2-9	Multistar 4830 back-EMF waveform . . . . .	20
3-1	Schematic of 3-phase inverter . . . . .	24
3-2	Center-aligned PWM with synchronized current sampling. The top three traces are high-side gate drive signals, while the bottom trace is the current sampling period. . . . .	25
3-3	Motor driver hardware . . . . .	25
3-4	Velocity by naive differentiation . . . . .	28
3-5	Velocity by edge-timing . . . . .	28
4-1	Bode plot of controller, plant, and return ratio . . . . .	31
4-2	Predicted vs. measured q-axis step response . . . . .	31
4-3	Modified PD controller block diagram . . . . .	33
4-4	Torque vs rotor angle and current . . . . .	34

5-1	Motor module . . . . .	37
5-2	Motor module section view with some features highlighted . . . . .	38
5-3	Planet and planet carrier design . . . . .	39
5-4	Exploded view of gearbox assembly . . . . .	39
6-1	Leg range of motion . . . . .	41
6-2	Actuator torque required for vertical force of 12 times leg assembly mass	42
6-3	Leg and linear guide assembly . . . . .	43
6-4	Timeseries of a single jump . . . . .	43

# List of Tables

2.1	.....	20
-----	-------	----



# Chapter 1

## Introduction

### 1.1 Motivation

The recent growth of the hobby remote-controlled airplane and multirotor market has produced great availability of very low-cost yet torque and power dense brushless electric motors. However, these motors have been for the most part neglected by the robotics community, at least for purposes other than open-loop spinning of propellers or similar loads.

Of particular interest, these motors can be found in large airgap radius, short length geometries, making them well suited for use in low transmission ratio, highly backdriveable robotic legs [2]. Given well matched motor control hardware capable of torque and position control, with these actuators it should be possible to build robots capable of dynamic locomotion at significantly reduced cost, compared to actuator systems presently used, without sacrificing performance.

### 1.2 Scope

This thesis documents the construction of a 2 degree of freedom robotic leg, using low-cost RC multirotor motors for actuators. This includes characterization and selection of specific motors, design of an inverter and motor control system, design of a single-stage planetary gearbox, and integration of these elements into a single motor module,

shown in Figure 1-1-a. Two of these motor modules were used to build a planar two degree of freedom leg, as shown in Figure 1-1-b.

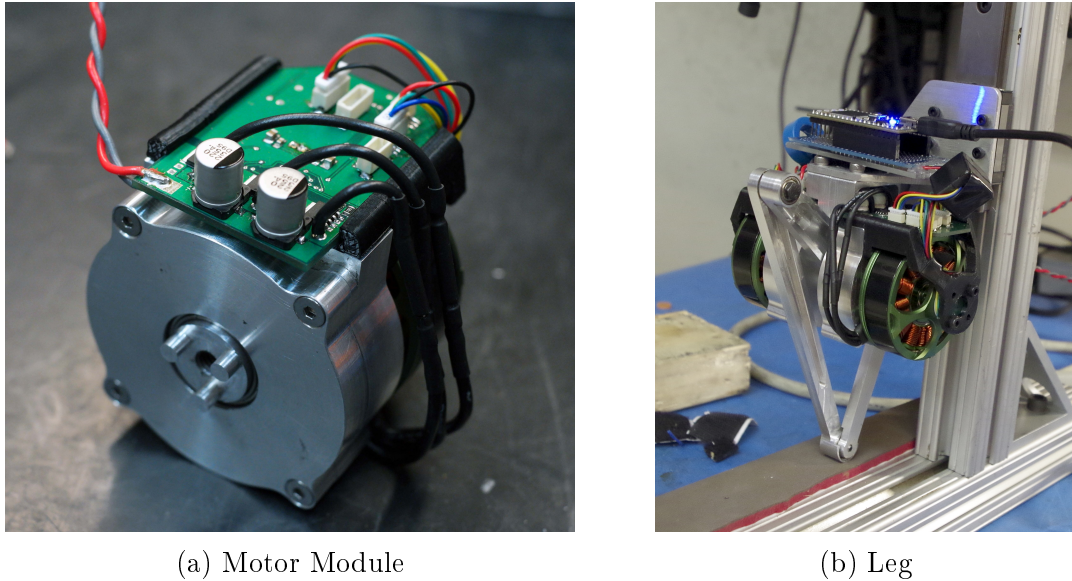


Figure 1-1: Motor module and 2-DOF Leg

### 1.3 Thesis Organization

The organization of this thesis is as follows:

- **Chapter 2** details the characterization and selection of motor candidates.
- **Chapter 3** describes design of the power electronics and hardware for motor control.
- **Chapter 4** describes the motor control algorithms used for motor commutation, sensing, and position and impedance control.
- **Chapter 5** covers the integration of motor, electronics, and single-stage planetary gearbox into a single unit.
- **Chapter 6** describes the integration of two motor modules in a two degree of freedom leg capable of jumping.

- **Chapter 7** summarizes the system developed, and suggests further work and improvements.



# Chapter 2

## Motor Characterization and Selection

A wide selection of hobby motors are available in the size and cost range of interest. A number of these were selected visually based on their geometry (large airgap radius, short length) and cost, and characterized to determine their suitability for legged robots. Figure 3 shows the array of motors examined



Figure 2-1: Selection of motors tested.

### 2.1 Testing Methodology

To characterize their performance to first order, several parameters were measured for each motor. Torque constant was estimated by observing the line-to-line back-emf on an oscilloscope, while spinning the motor at a constant velocity. Line-to-line resistance of the three phases of each motor was measured by 4-wire measurement, and each motor was weighed. While these parameters far from fully describe the

performance of each motor, they give decent insight to how much torque each motor can produce and how efficiently they use magnetic material.

## 2.2 Measurement and Characterization

### 2.2.1 Turnigy 5208 Gimbal Motor

This motor was designed for camera gimbals, so is wound for a high torque constant and built for low-speed operation. Its mechanical design is lacking, with small shaft and bearings, no rotor balancing features, thick stator laminations, messy windings, and poor slot fill factor.



Figure 2-2: Turnigy 5208 Gimbal Motor

Torque constant according to back-EMF measurement (See Figure) is  $0.3081 \text{ N}\cdot\text{m}/\text{A}$ , and resistance was measured to  $11.7 \Omega$ . This gives a motor constant of  $0.0901 \text{ N}\cdot\text{m}/\sqrt{\text{W}}$ . Peaks in the back-EMF waveform are noticeably sharper than a pure sinusoid.

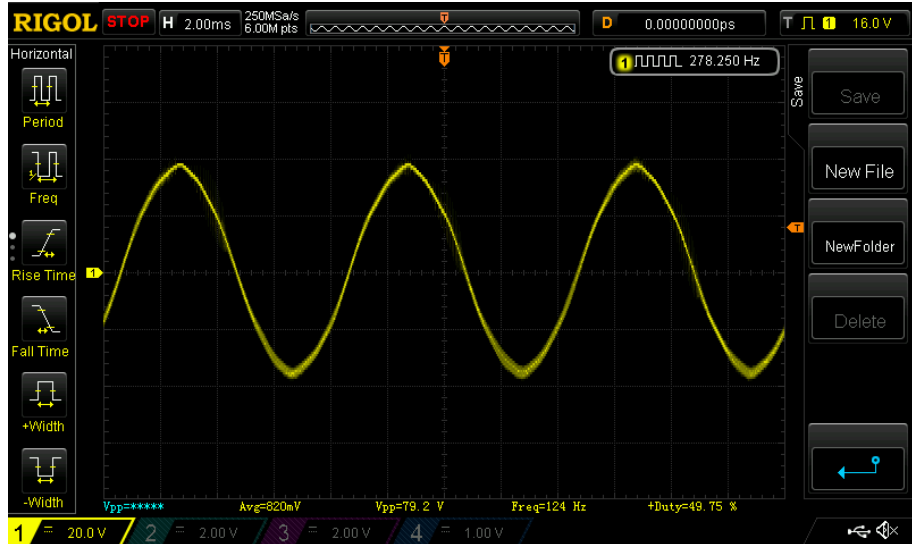


Figure 2-3: 5208 Gimbal Motor back-EMF waveform

### 2.2.2 Turnigy 5010 Multistar Elite

The Multistar Elite is of excellent build quality, with neat, single strand windings (although fill factor is still rather poor), curved N45SH magnets rather than the rectangular ones typically used in hobby motors, large bearings and shaft, and much thinner stator laminations than the gimbal motor.



Figure 2-4: Turnigy Multistar Elite 5010

Torque constant according to back-EMF measurement (See Figure) is 0.0333 N·m/A, and resistance was measured to 128 mΩ. This gives a motor constant of 0.09304 N·m/ $\sqrt{W}$ . The appearance of the back-EMF waveform is between trapezoidal and sinusoidal.

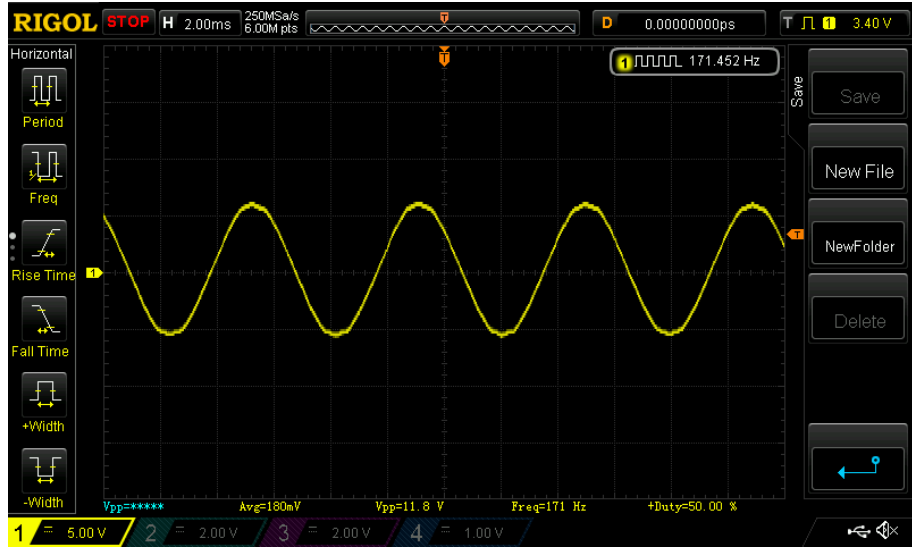


Figure 2-5: MultistarElite 5010 back-EMF waveform

### 2.2.3 Gartt ML 5208

The Gartt motor has 11 pole pairs, rather than 7 like the previous two motors. More poles can mean better torque density: Because there is less magnetic flux between stator teeth and between poles in the back iron of the rotor, steel in these areas can be made thinner. However, the performance of the Gartt did not stand out compared to the 7 pole-pair motors, and in fact had inferior performance. Mechanical construction quality is generally good, although there are large gaps between adjacent magnets on the rotor.



Figure 2-6: Gartt 5208 Motor

Torque constant according to back-EMF measurement (See Figure) is 0.02498 N·m/A, and resistance was measured to 98 mΩ. This gives a motor constant of

$0.0800 \text{ N}\cdot\text{m}/\sqrt{W}$ . The back-EMF waveform is noticeably less sinusoidal than the previous two motors.

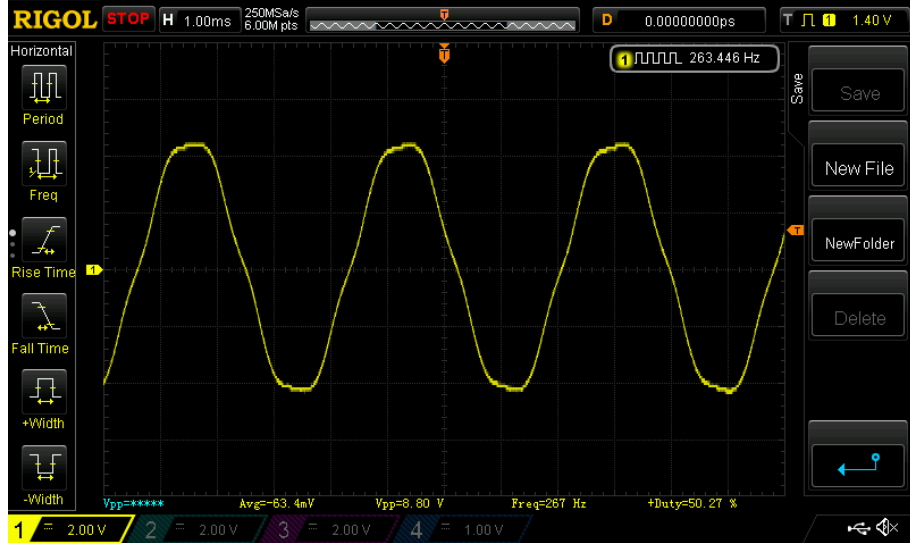


Figure 2-7: Gartt 5208 back-EMF waveform

#### 2.2.4 Turnigy Multistar 4830

The Multistar 4830 has a longer aspect ratio than the other motors tested, and 11 pole pairs, like the Gartt.



Figure 2-8: Turnigy Multistar 4830

Torque constant according to back-EMF measurement (See Figure) is  $0.0212 \text{ N}\cdot\text{m}/\text{A}$ , and resistance was measured to  $103 \text{ m}\Omega$ . This gives a motor constant of  $0.0662 \text{ N}\cdot\text{m}/\sqrt{W}$ . The back-EMF waveform contains a very noticeable 5th harmonic.

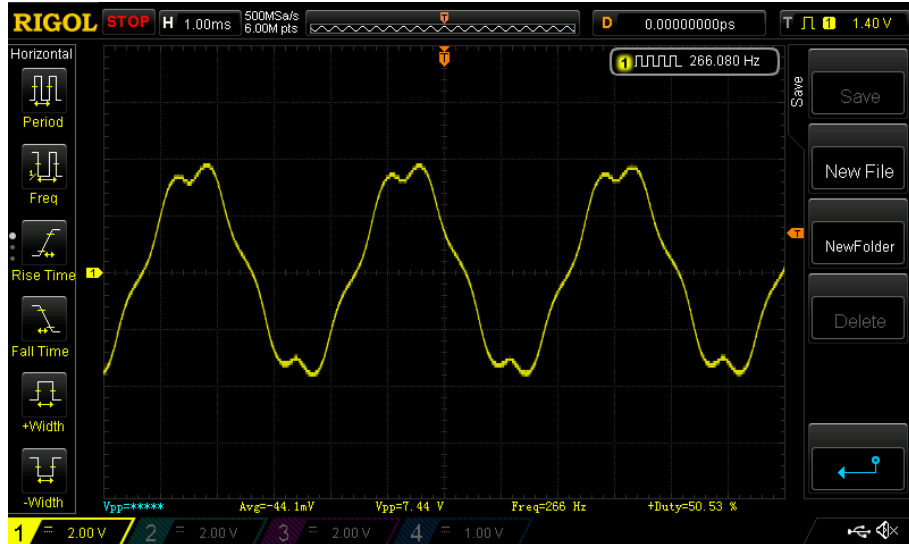


Figure 2-9: Multistar 4830 back-EMF waveform

## 2.3 Testing Conclusions and Motor Selection

Results of the motor characterization, including mass and cost (at the time of writing) each motor, are summarized in the following table.

Model	Torque Constant (N·m/A)	Resistance (mΩ)	Motor Constant (N·m/ $\sqrt{W}$ )	Mass (g)	Cost (\$)
Gimbal 5208	0.3081	11,700	0.0901	167	39.2
Multistar Elite 5010	0.0333	128.0	0.0930	183	52.69
Gartt 5208	0.02498	97.5	0.0800	173	40.00
Multistar 4830	0.0212	102.8	0.0662	162	43.29

Table 2.1

From the results of this testing, the Multistar Elite 5010 motor was chosen. While its cost is slightly greater than the other motors tested, its construction quality is much

better, and performance slightly higher. Additionally, thanks to a sale, most of the motors used were purchased at \$42.15, making them almost identically priced to the other motors tested.



# Chapter 3

## Motor Control Hardware

To achieve the desired motor performance, a custom motor controller was developed with the following functional requirements in mind:

- Light weight and small form factor: 10's of grams, physically smaller than the motor.
- Current: 15 A continuous current, 40 A peak fraction-of-a-second bursts, with minimal heatsinking.
- Up to 24 V input voltage.
- Capable of torque/position/impedance control.

### 3.1 Inverter

A 3-phase inverter was designed, capable of driving the desired current with minimal cooling. The bridge was built from 40 V,  $2.5\text{ m}\Omega$  MOSFETs with low (35 nC) gate charge, for low power dissipation switching at rated current.

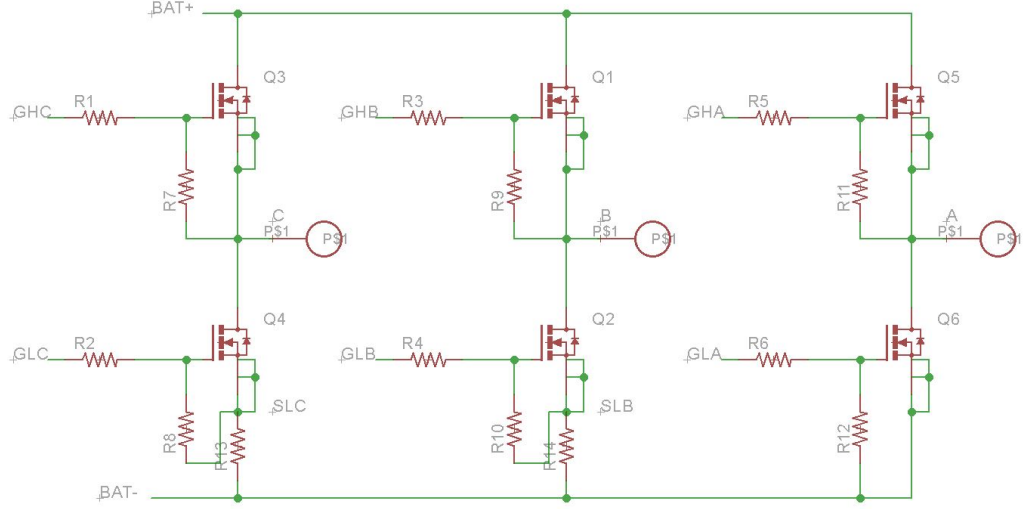


Figure 3-1: Schematic of 3-phase inverter

Gate drive of the MOSFETs was accomplished with the TI DRV8302 IC. In addition to 3-phase gate drive, this IC conveniently also has a built in buck converter (sans-passives) for logic power, and a pair of current sense amplifiers to boost the voltage drop across the low-side current shunts. Use of this chip greatly simplified design and layout of the controller. The motor control algorithm runs on an STM32F446 microcontroller.

For current sensing, low-side (between the source of the low-side transistor and ground) shunts were used on two of the three phases. Only two out of three phases are required; because the current into the three phases must sum to zero, the third current can be calculated from the other two. While low-side current shunts makes amplification of the voltage drop across the shunt easy (the amplifier can be ground referenced, and does not need to be differential), current only flows through the shunt while the low-side transistor is closed. To get valid current measurements from this topology, the microcontroller must be configured to sample only while the low-side transistor is closed. This strategy has the added benefit of avoiding switching transients during current sampling, which could introduce noise into the measurement.

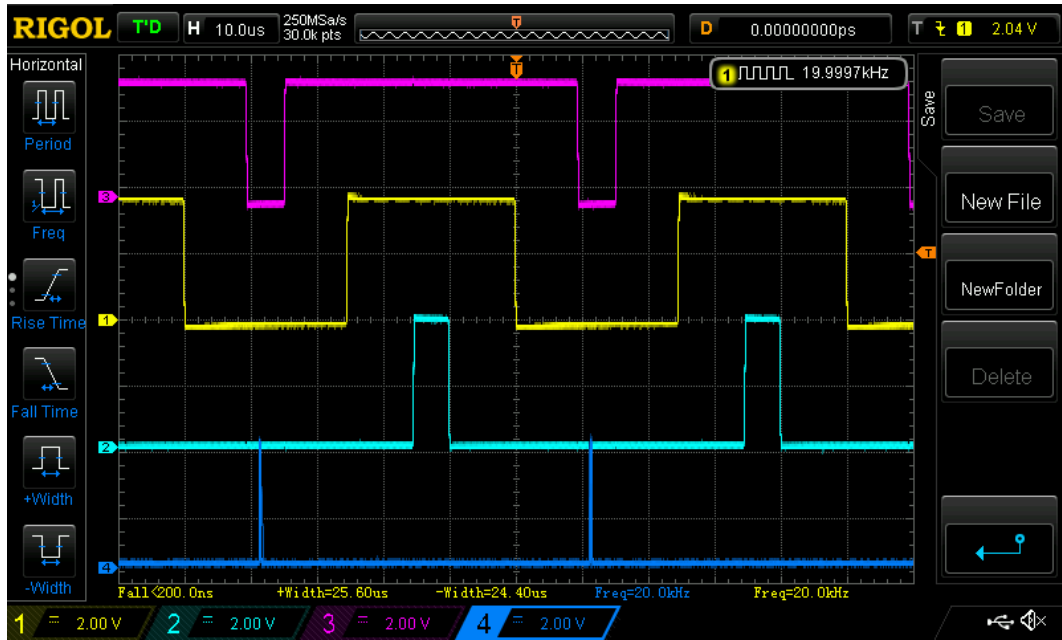


Figure 3-2: Center-aligned PWM with synchronized current sampling. The top three traces are high-side gate drive signals, while the bottom trace is the current sampling period.

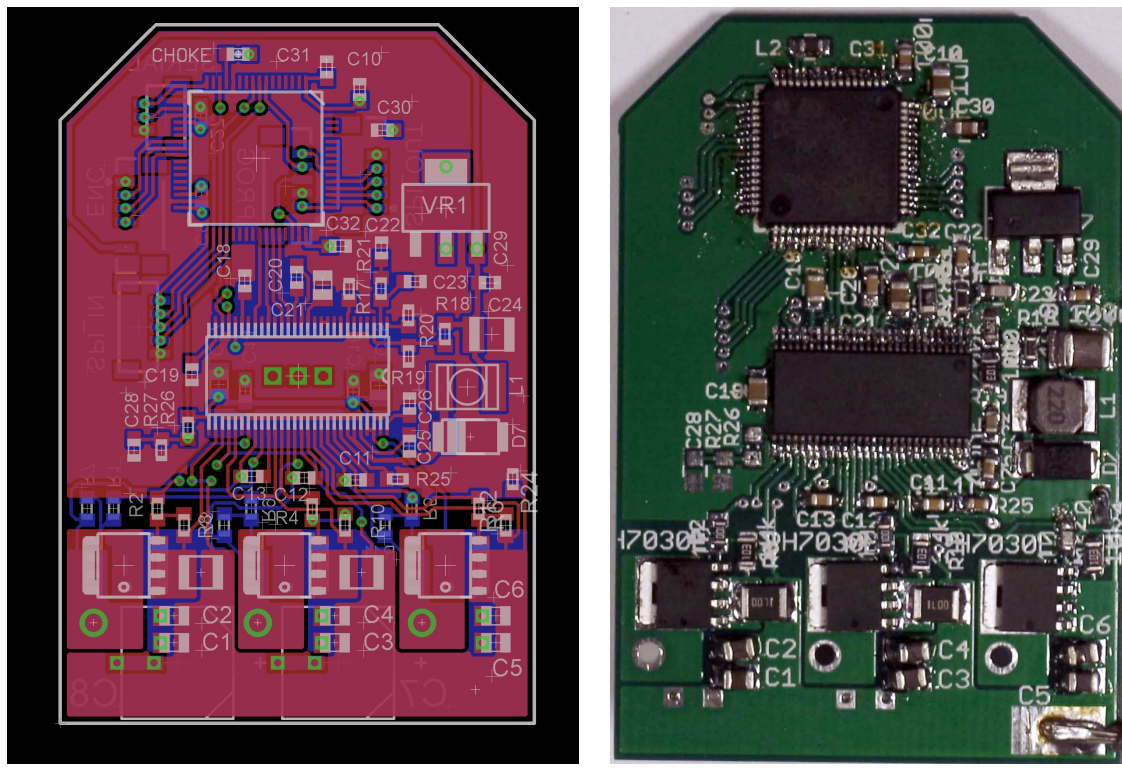


Figure 3-3: Motor driver hardware

## 3.2 Position and Velocity Sensing

Position and velocity sensing are critical for both motor commutation and position/impedance control of joints, so substantial effort was put into researching and testing different position sensors. The two categories of position sensor investigated were optical encoders, and absolute hall-effect array based position sensing integrated circuits. Eventually an absolute hall-effect sensor was chosen for its combination of low costs, small size, and absolute measurement.

### 3.2.1 Hardware

The specific position sensor chosen was the MagAlhpa MA700. This sensor features 11-bit position resolution, 500 kHz refresh rate, and only  $3\mu\text{s}$  latency. The IC is paired with a diametrically magnetized cylindrical magnet on the motor shaft. Absolute position is read from the sensor over an SPI interface. Additionally, the IC provides a 10-bit encoder output, with quadrature channels and an index pulse.

Initially, the magnet is randomly aligned with the rotor, so one-time calibration must be done to determine the position offset of the sensor with respect to the electrical position of the rotor. To do so, the rotor is aligned with the d-axis by applying a voltage to phase A, and grounding phases B and C [3]. The angle measured at this point is used as the zero angle.

### 3.2.2 Velocity Measurement Technique

Accurate velocity measurement is important for motor control (in the feed-forward decoupling path, as will be discussed in the next chapter) as well as damping control. However, estimating velocity using a position sensor can be challenging. The naive approach of differentiating and filtering position measurement is often unsatisfactory. Inherently, the derivative operation amplifies high frequency components of a signal, and becomes especially problematic for quantized signals (whether natively quantized like an encoder or by an A/D converter).

An alternative velocity estimation scheme is to time the transitions between position sensor states. The period between changes in position sensor output will be inversely proportional to angular velocity. With any position sensor, this can be achieved by sampling the sensor much faster than the minimum time between state-changes. However, this process is especially convenient with an encoder-type sensor, which outputs a digital signal upon state change. Two timers of the STM32F4 microcontroller were configured to automatically keep track of the count of the encoder, and store the number of clock cycles in between encoder edges. This way, the period between encoder edges could be measured without the need for a very fast loop constantly sampling the position sensor.

Examples of velocity estimate for a 40 rad/s velocity reference with a 11-bit position sensor and 10 kHz sample rate are shown below, for both naive differentiation and edge-timing methods.

In the case of differentiated position signal, for most samples, the change in sensor output is zero, so velocity estimate is zero. The most the output of the sensor ever changes in one sample period is a single bit. While low-pass filtering of this signal can be done, the phase-lag caused becomes significant once the filter is slow enough to adequately smooth the signal.

By comparison, the velocity estimate by edge-timing much more closely matches actual velocity. At low-speed, the estimate gets worse, as the frequency of edges decreases. Performance can be further improved by extrapolation velocity estimates from previous samples, in between edges.

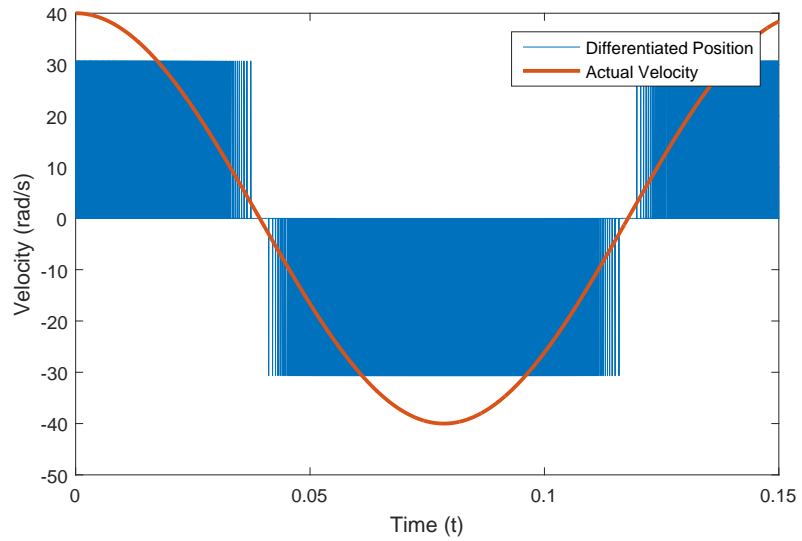


Figure 3-4: Velocity by naive differentiation

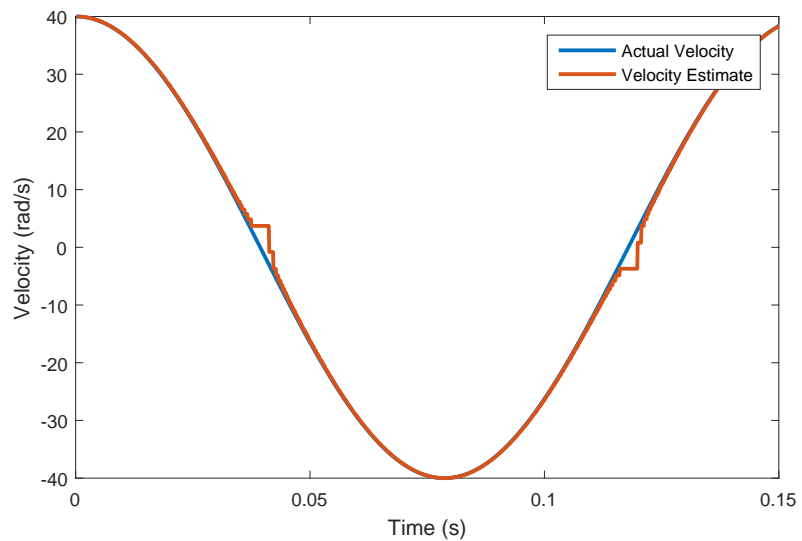


Figure 3-5: Velocity by edge-timing

# Chapter 4

## Motor Control

The high-level motor control approach taken was to control joint position and impedance. To achieve this, a multi-level approach was taken to control. An impedance controller takes inputs of position, stiffness, and damping, and outputs actuator torques required to achieve said parameters. A torque controller converts motor torque into d and q-axis currents. These currents are fed into a field-oriented control implementation, which regulates motor currents to achieve the desired performance.

### 4.1 Field Oriented Control Implementation

A detailed description of Field Oriented Control (FOC) is beyond the scope of this thesis, but the principle is as follows. Rather than directly control sinusoidal currents (or other waveforms) onto the phases of the motor, a coordinate transformation (the dq0 transform) is performed on the measured phase currents, to map the currents to a coordinate system which rotates with the rotor. Stator current in this reference frame has components along two axes, the quadrature (q) axis, which is orthogonal to the magnetization of the rotor, and direct (d) axis, which is aligned to the magnetization of the rotor. For a surface-permanent magnet rotor, to produce maximum torque-per-amp, all current should be placed on the q axis, and the d axis current should be controlled to zero. Control is performed the d-q reference frame. The controller outputs are then passed through the inverse dq0 transform to map them back into

phase voltages which are applied to the motor.

This scheme is appealing, because torque is controlled by a single value, q axis current, rather than three phase current. Further more, in steady state, q and d currents are constants, rather than time-varying like phase currents, so the bandwidth of the current controller does not need to be high - it only determines the bandwidth of torque response.

#### 4.1.1 Current Regulator Design

To control d and q axis current, independent discrete-time PI controllers are used, with a feed-forward path to decouple the d and q axes. Because the motor used has permanent magnets on the surface of the rotor, its d and q axis inductances are the same. Therefore only one current controller was designed, and implemented on both axes.

Using a measured d/q axis inductance of  $33\mu\text{H}$ , phase resistance of  $192 \text{ m}\Omega$  and sample rate of  $10 \text{ kHz}$ , a conservative current controller with a crossover frequency of  $3,850$  radians per second and  $51.6$  degrees of phase margin was designed and implemented. While both sample rate and crossover could be pushed higher, for the purpose of getting the system working, faster current response was not required and design was kept conservative to avoid instability and damage to hardware in the case of modeling errors.

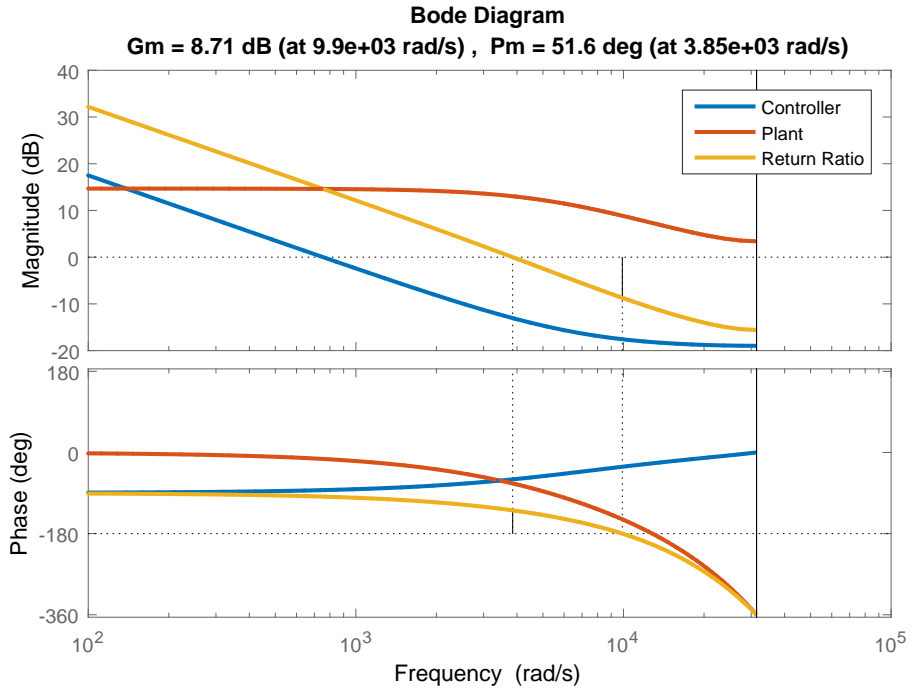


Figure 4-1: Bode plot of controller, plant, and return ratio

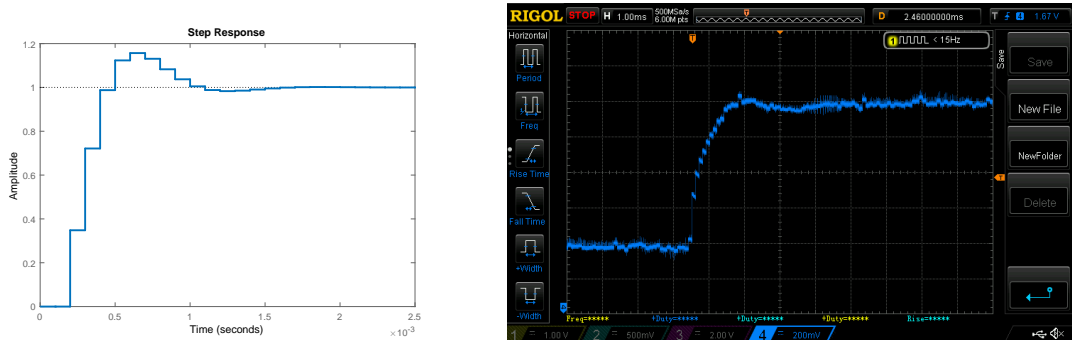


Figure 4-2: Predicted vs. measured q-axis step response

The current regulator design discussed above assumes that the d and q axes are independent of one another. However, the d and q axis voltages are actually coupled. To decouple the two systems, so that the current regulators perform as expected, a feed-forward decoupling path should be implemented.

q and d axis volages are given by the following expressions, with coupling terms in bold:

$$V_d = i_d R + L \frac{di_d}{dt} + \omega \mathbf{L} \mathbf{i}_q \quad (4.1)$$

$$V_q = i_q R + L \frac{di_q}{dt} - \omega \mathbf{L} \mathbf{i}_d + \omega K_e \quad (4.2)$$

Where  $i_d$  and  $i_q$  are d and q axis currents,  $R$  is resistance,  $L$  is inductance,  $\omega$  is electrical frequency, and  $K_e$  is the Back-EMF constant [1].

The coupling terms are proportional to the inductance, (electrical) angular velocity, and d/q axis currents. To cancel out the coupling terms, these quantities are subtracted from the outputs of the d and q axis current regulators. Since torque response has so far only been measured in a static case, the effect of decoupling has not yet been quantified for these motors, but it should improve speed and accuracy of torque response at speed.

## 4.2 Torque and Impedance Control

As presently implemented, the torque controller is simply a static gain of the inverse torque constant of the motor. However, it is a placeholder for techniques such as cogging torque and torque ripple compensation which will be implemented in the future.

Pseudo-impedance control is achieved through a simple PD position controller. The controller takes reference, stiffness, and damping inputs, and outputs a torque command. The proportional constant is analogous to torsional spring constant - this part of the controller commands a torque proportional to the displacement of the motor from its reference position. The derivative term is analogous to the damping coefficient of a dashpot - this part of the controller commands a torque proportional to the velocity difference between the reference and motor. Neglecting the inertia and friction of the motor and gearbox, these controller parameters specify the joint impedance. Since due to mechanical design, the inertia and friction are small (compared to typical robotics actuators with large gear ratios), they only affect the impedance of the the joint at high frequencies (such as ground impacts, for a leg),

and good impedance response can be achieved everywhere else.

For the purpose of implementation, the control scheme outline above was slightly modified. Rather than differentiate error signal for the derivative term, which is a typical way to implement a PD controller, the error derivative is replaced by the motor angular velocity. For a step input or constant position reference, these controllers behave identically. However, for a position reference with a defined slope, using motor velocity adds extra damping related to the derivative of the position reference. This approach was taken to avoid noise introduced by differentiating the discrete position reference. However, a "correct" PD controller could be implemented without differentiation, by adding a fourth input of velocity reference.

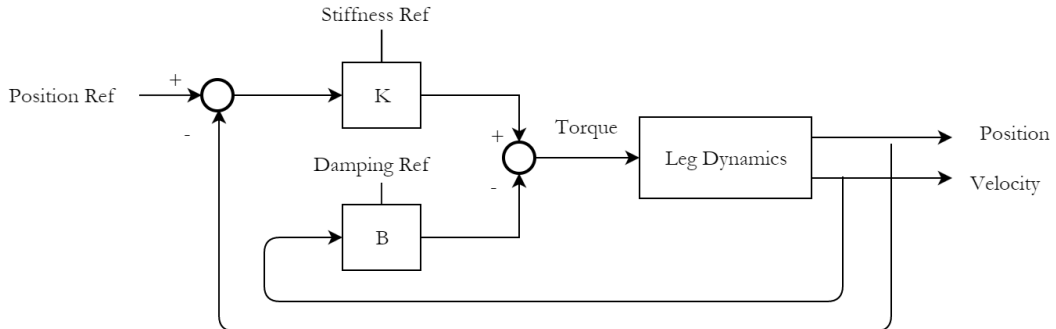


Figure 4-3: Modified PD controller block diagram

### 4.3 Measurement of Cogging Torque and Torque Ripple

To examine the motor performance and determine the necessity for cogging torque and torque ripple compensation, the static torque of the motor with controller was measured as a function of rotor angle and q-axis current. To accomplish this, the output of a motor was coupled to an S. Himmelstein 4901V rotary torque transducer. The other input to the torque transducer was coupled to an indexing head, which allowed the shaft to be slowly rotated. Torque data from the sensor and angle data from the motor controller were streamed to a computer and recorded.

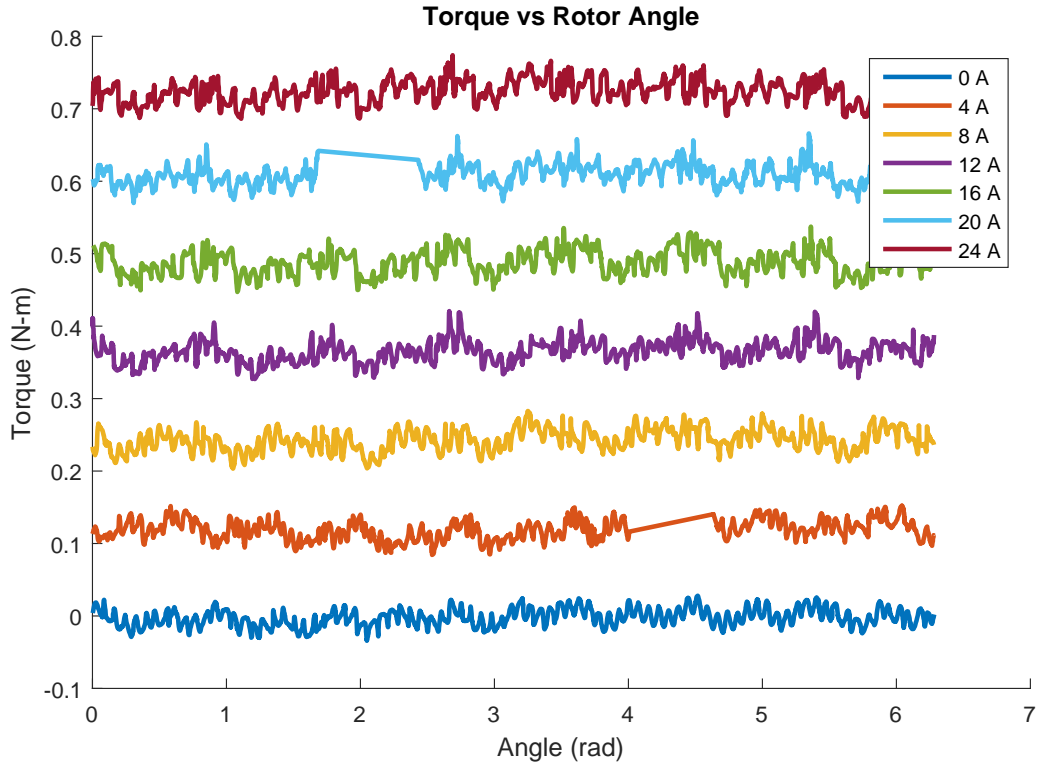


Figure 4-4: Torque vs rotor angle and current

Cogging torque, as shown in the 0 A trace in the above figure, shows components at electrical frequency (seven cycles per mechanical rotation) as well as higher-frequency components. Maximum cogging torque amplitude is .025 N·m. Overall amplitude of torque ripple did not change significantly between zero and 24 amps, although the ripple at high current shows noticeably sharper peaks.

With a measurement of cogging torque vs. rotor angle, cogging torque could be easily feed-forward compensated in the future, to improve torque control accuracy and reduce vibrations, etc. A simple lookup table would specify the required q axis current required to cancel cogging, as a function of rotor angle. This current would simply be added to the output of the q axis current regulator.

The torque constant measured during this testing is lower than that predicted by measurement of the motor's back-EMF. Measured torque constant was 0.031 N·m/A, compared to a predicted value of 0.0384. A possible explanation for this error is incorrect alignment of the position sensor with the orientation of the rotor.





# Chapter 5

## Motor Module Design

The motor, motor control, and position sensing system outlined in the previous chapters was integrated into an all-in-one motor module with a single-stage planetary gearbox on the output.. This module could be a building block for robotic legs, arms, or other systems requiring a lightweight, power and torque dense motor system with low mechanical impedance.

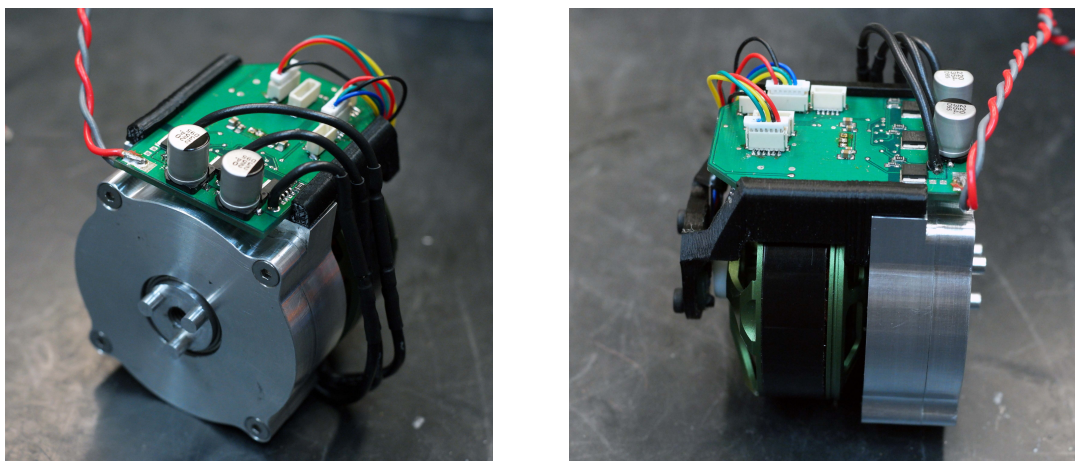


Figure 5-1: Motor module

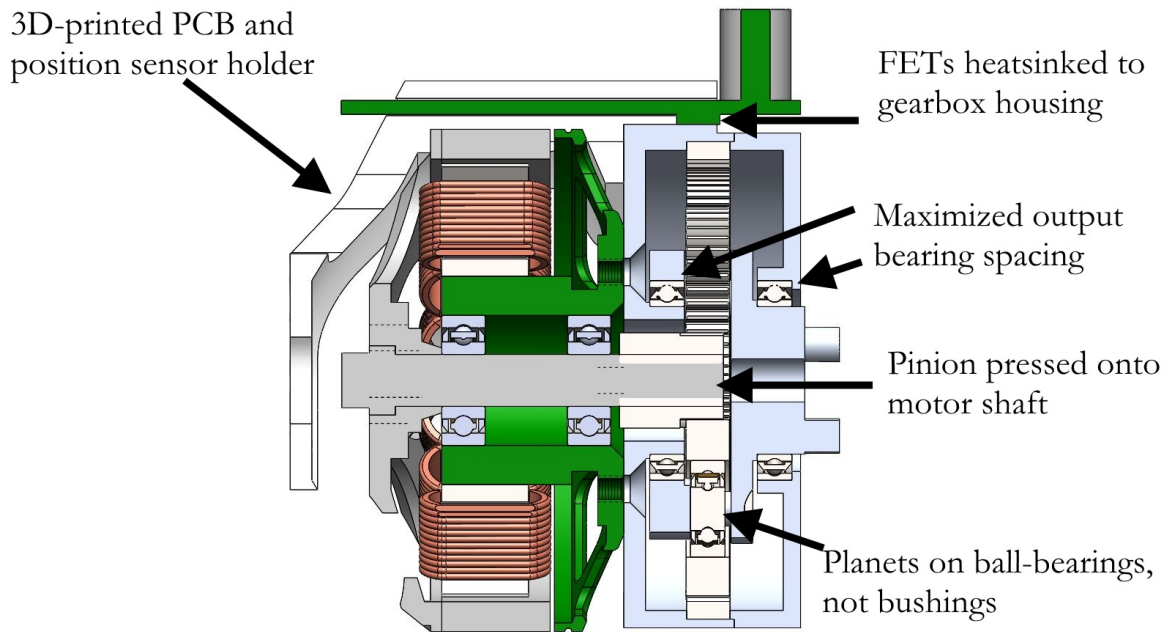


Figure 5-2: Motor module section view with some features highlighted

A low-backlash, low-friction single-stage planetary gearbox was designed to couple to the output of the motor. Additionally, the gearbox was designed to have a leg singly-supported by the output shaft. Gearbox weight was minimized wherever possible. Due to these design criteria, the mechanical design of the gearbox differs somewhat from typical planetary gear reductions.

To maximize bearing spacing of the output shaft, to support leg directly attached to the output, a two-part planet carrier was designed. The two halves of the carrier are aligned by interference fits of the three planet-supporting posts. For simple attachment of a leg to the output, the carrier was designed with 3 torque-transmitting pins on the output, with a central tapped hole. A single bolt can be used to attach a leg to the output of the gearbox. Torque is transferred by a combination of shear of the pins and friction from bolt clamping force. The pins were sized such that they can withstand 9 times peak motor torque, even without any clamping pressure from the central bolt.

To reduce gearbox backlash and friction, each planet gear rides on a ball bearing

press-fit into its center, rather than on a plain bearing, as is typical. These bearings were sized to be able to carry the output torque of the motor/gearbox assembly.

The gearbox housings and planet carrier parts were CNC machined from 6061 T6 aluminum. The .5 module, 5mm facewidth gears were donated by KHK Gears, and required some manual modification for this gearbox design. The 40 tooth planets were bored out and pressed with bearings, and the outer diameter of the 100 tooth ring gear was turned down substantially. The bore of the 20 tooth pinion was reamed undersized and press fit onto the 6mm motor shaft.

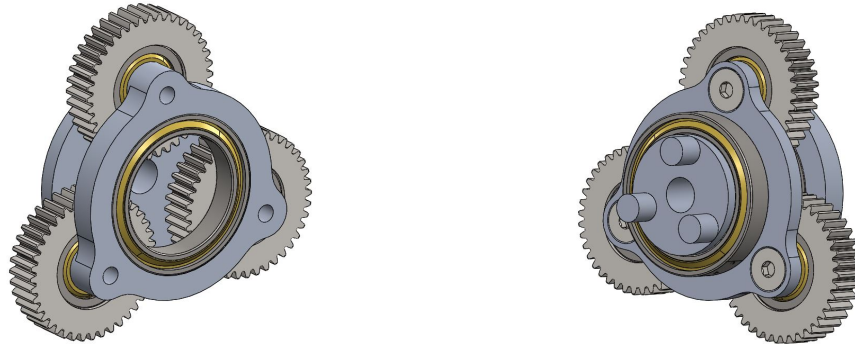


Figure 5-3: Planet and planet carrier design

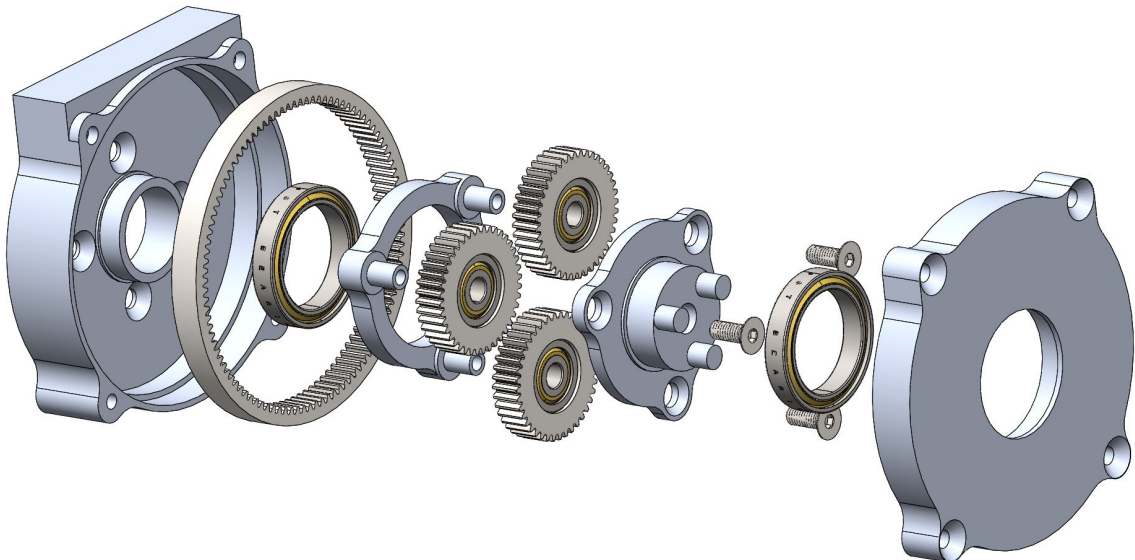


Figure 5-4: Exploded view of gearbox assembly

The final gearbox assembly has a total reduction of 6:1, and mass of 120 grams,

or roughly 2/3 the mass of the motor. The entire motor module, including position sensor and inverter, has a mas of under 350 grams, should be able to produce 7.4 N·m of torque at 40 amps (although effects of motor saturation have not yet been measured up to this point, so this number could be slightly reduced), and has a total output inertia of 1.02 g·m<sup>2</sup>.

# Chapter 6

## Two Degree of Freedom Leg

A simple two degree of freedom leg was built around a pair of the motor modules described in the previous chapter. A four-bar, parallel link leg configuration was used, with motors mounted co-axially at the hip of the leg. The lengths of the leg-links were chosen to be similar to those of the SMC robot, a small, relatively low-cost quadruped capable of dynamic gaits [4]. The links themselves were designed to be light-weight and provide a wide range of motion. Total extension of the leg (possible change in leg length) is 134mm, and nearly 180 degrees of rotation at full leg-extension is possible. Leg links were CNC machined from aluminum. Total leg mass, including links, bearings, and fasteners, was only 90 grams - less than half the mass of a single motor.



Figure 6-1: Leg range of motion

To verify the leg geometry, a MATLAB simulation was run to determine the actuator torques required for different ground forces. With a maximum actuator torque of 7.4 N·m, the leg can easily generate its weight in vertical force over its entire workspace. Furthermore, the leg can generate 12 times its total weight (or 3 times the total weight of a qudruped built from four such leg assemblies) over most of its workspace.

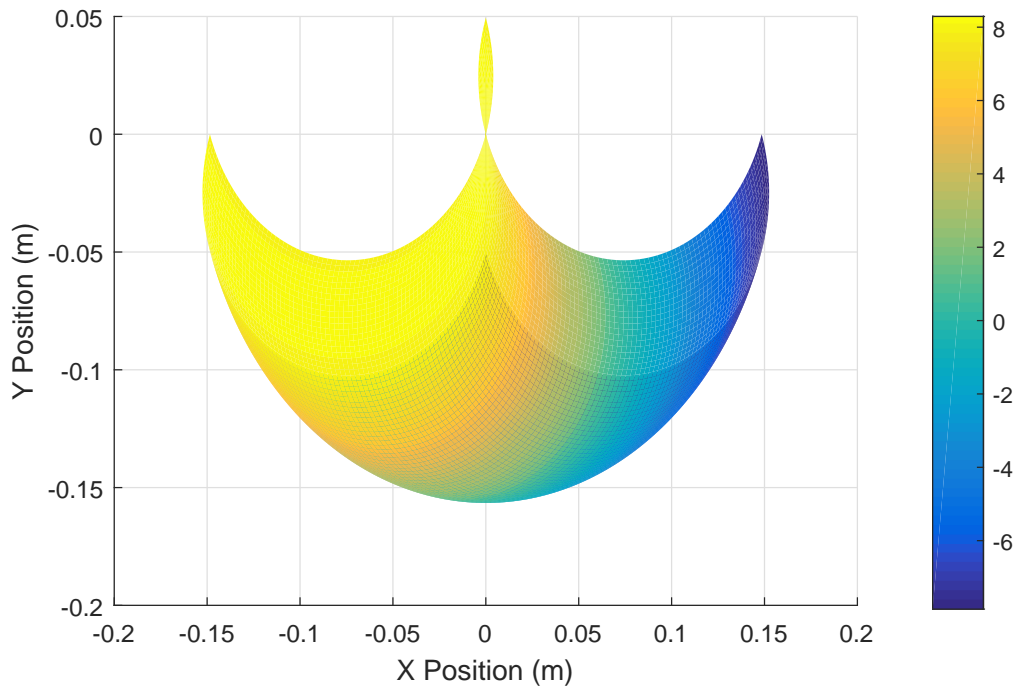


Figure 6-2: Actuator torque required for vertical force of 12 times leg assembly mass

To demonstrate jumping, the leg was constrained to vertical motion by a linear guide.

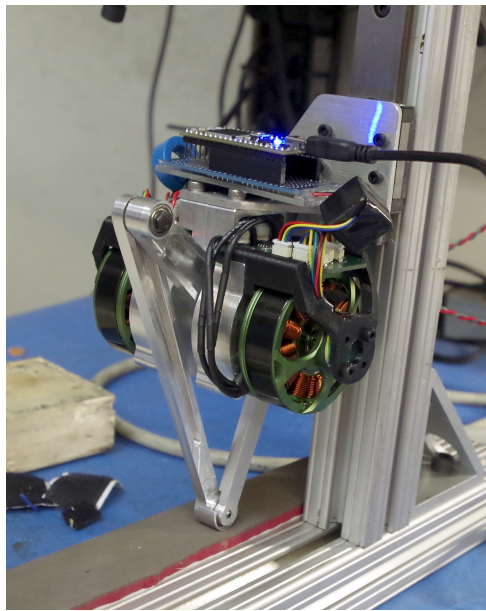


Figure 6-3: Leg and linear guide assembly

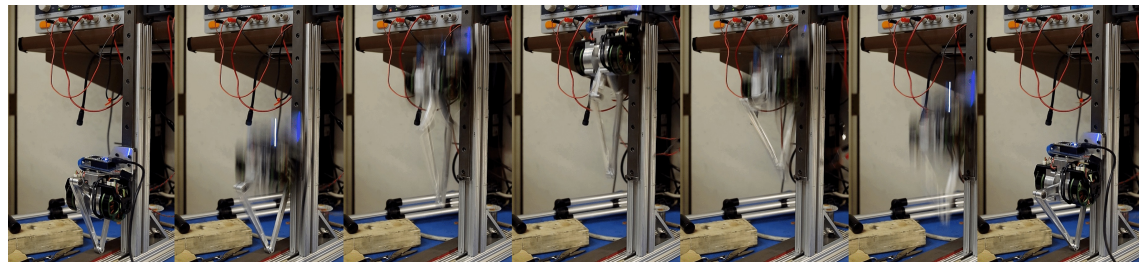


Figure 6-4: Timeseries of a single jump



# Chapter 7

## Summary and Conclusion

### 7.1 Design Summary

This thesis documents the development of the hardware and control architecture for the use of low-cost brushless motors, designed for the hobby remote-control vehicles market, in dynamic robots. Field-oriented control of current, and position/impedance control of said motors was implemented on custom motor control hardware, designed specifically for this application. A motor module was developed incorporating motor, electronics, and low-impedance planetary gearbox into a single unit, which can be used to build robotic legs or similar. Finally, a pair of motor modules was used to build a two degree of freedom leg, capable of jumping.

Hopefully the effort put into designing this system will help to lower the barrier to building high performance dynamic robots, by making the hardware cheaper, and designs and methods freely available.

### 7.2 Improvements and Future Work

A number of features should be added and changes should be made in future revisions of the hardware and firmware developed.

In the motor control firmware, the frameworks is already in place to do cogging torque compensation. However, before implementation, more sensitive measurement

of cogging torque should be performed with a higher resolution torque sensor.

Communication with each motor unit needs improvement. Current transients from the motor controller cause the ground of each motor controller to change with respect to the computer sending commands, which has caused numerous communication problems. More robust communication protocol and hardware (isolated and/or differential) , and improved PCB layout should be used to alleviate this issue.

For attaching the motor control and position sensing PCBs to the motor unit, a more robust solution than the 3D-printed mount should be used. Ideally, the position sensing IC could be integrated into the motor control board, rather than separate and connected by cables, and the motor controller placed directly behind the motor.

# Bibliography

- [1] András Zentai, Tamás Dabóczki *Improving Motor Current Control Using Decoupling Technique* EUROCON 2005
- [2] Sangok Seok, Albert Wang, David Otten and Sangbae Kim. *Actuator Design for High Force Proprioceptive Control in Fast Legged Locomotion* IEEE, 2012.
- [3] Viktor Bobek *PMSM Electrical Parameters Measurement* Freescale Semiconductor Application Note, 2013
- [4] Will Bosworth, Michael Farid, Deborah Ajilo, Sangbae Kim, and Neville Hogan *Bounding, jumping, turning and stopping with a small, low-cost quadrupedal robot* Massachusetts Institute of Technology, 2015.